Tarisciotti, Luca and Lei, Jiaxing and Formentini, Andrea and Trentin, Andrew and Zanchetta, Pericle and Wheeler, Patrick and Rivera, Marco (2018) Modulated predictive control for indirect matrix converter. IEEE Transactions on Industry Applications . ISSN 1939-9367

Modulated Predictive Control for Indirect Matrix Converter

Luca Tarisciotti, Andrea Formentini , Andrew Trentin, Pericle Zanchetta, Patrick Wheeler
Department of Electrical and Electronics Engineering
The University Of Nottingham, Nottingham, UK
luca.tarisciotti@nottingham.ac.uk

Jiaxing Lei
College of Automation Engineering
Nanjing University of Aeronautics and Astronautics Nanjing, Jiangsu, China
ljxnuaa@nuaa.edu.cn

Marco Rivera
Universidad de Talca
Department of Electrical Engineering
marcoriv@utalca.cl

***Abstract*— Finite State Model Predictive Control (MPC) has been recently applied to several converter topologies as it can provide many advantages over other MPC techniques. The advantages of MPC include fast dynamics, multi-target control capability and relatively easy implementation on digital control platforms. However, its inherent variable switching frequency and lower steady state waveform quality, with respect to standard control which includes an appropriate modulation technique, represent a limitation to its applicability. Modulated Model Predictive Control (M²PC) combines all the advantages of MPC with the fixed switching frequency characteristic of PWM algorithms. The work presented in this paper focuses on the Indirect Matrix Converter (IMC), where the tight coupling between rectifier stage and inverter stage has to be taken into account in the M²PC design. This paper proposes an M²PC solution, suitable for IMC, with a switching pattern which emulates the desired waveform quality features of Space Vector Modulation (SVM) for matrix converters. The switching sequences of the rectifier stage and inverter stage are rearranged in order to always achieve zero-current switching on the rectifier stage, thus simplifying the current commutation strategy.**

Keywords—Indirect Matrix Converter (IMC), Modulated Model Predictive Control (M²PC), Predictive Control, AC-AC power conversion.

I. INTRODUCTION

Matrix converters have often been considered as an alternative to more traditional topologies due to their advantage of offering direct AC-AC power conversion without the need of an intermediate DC link energy storage. Matrix converters can minimize the size of the required passives components, thus increasing the potential power density and reliability of the converter[1], [2]. For such reasons Matrix converters are often proposed in high power density applications, such as drive [3], [4], aircraft ground power supply units [5], inductive power transfer [6]–[8] and hybrid transformers [9], [10], as a compact alternative to standard back-to-back AC/AC topologies. Among all the possible topologies in the matrix converter family, the Indirect Matrix Converter (IMC) represents an interesting solution for direct AC-AC power conversion in many applications. The IMC is composed of a rectifier stage and an inverter stage which are directly connected, without DC link energy storage elements [11]–[13]. In order to modulate the AC waveform in the rectifier stage, bidirectional switches are required [14].

When compared to the Direct Matrix Converter (DMC), the IMC presents zero current switching on the input stage, which simplify the commutation of the bidirectional switches [11], while the output stage, which is always hard switched, does not present particular commutation issues. For such reason when the IMC is designed for high switching frequencies, taking advantage of modern Silicon Carbide (SiC) MOSFETs [15], the input stage bidirectional switches can still be achieved using standard IGBT silicon devices requiring only 6 SiC MOSFETs for the output stage. On the contrary, in the case of DMC, all 18 switches have to be realized using SiC MOSFETs [13]. Moreover, when the converter output frequency is similar to the input frequency, the IMC achieve a better losses distribution over all the switching devices than DMC. This can be achieved when IGBT devices are selected and advanced modulation schemes are implemented [16] or using a classical modulation scheme but SiC MOSFET devices on the output stage [17]. The IMC features bidirectional power flow, sinusoidal input and output currents, and controllable input power factor. The topology has been suggested as a potential alternative to conventional voltage source converters due to its advantages in terms of power density. For such reasons control strategies [18], [19], modulation algorithms [20]–[25], extended topologies [26] and applications for IMC [27]–[29] are often investigated. When compared to the traditional Back-to-Back converter, the IMC requires a higher number of power semiconductor devices.

In the IMC topology, a direct coupling between the converter input and output is present. As a result, the modulation algorithms and control strategy complexity is increased [20]–[22]. Space Vector Modulation (SVM) is widely applied to the IMC [30] where in every sampling period, the expected input current vector and output voltage vector are synthesized by applying multiple fundamental vectors. However, with the rapid development of digital processors and power devices, the use of SVM in conjunction with linear controllers is now being challenged by Model Predictive Control (MPC) [13].

MPC provides numerous advantages over conventional modulation and control methods, such as the capability of achieving several control targets within a single control loop, easy implementation on digital control boards, capability of include constraints in the control system and improved dynamic performance [3], [4], [31]–[34]. MPC has been successfully applied to the IMC to obtain sinusoidal input and output currents, control the input reactive power, increase efficiency and reduce common mode voltages [26], [28], [35], [36]. Considering all the possible switching states of IMC, MPC selects the best one to minimize a cost function in every sampling period. The cost function is usually composed by the difference between the predictions of the system variables to be controlled and their reference values. However, a critical issue of MPC is that, due to the lack of a modulator, only one switching state is applied to the converter in one sampling period. As a result, when compared to conventional PWM algorithms, MPC leads to larger ripple in the system waveforms [37]. Moreover, MPC presents a variable device switching frequency, thus resulting in a wide harmonic spectrum which extends from the fundamental frequency to half of the sampling frequency [27]. As a consequence, MPC requires a higher sampling frequency, with respect to linear controller with standard PWM algorithms, in order to achieve similar waveform quality, as well as increasing the input filter design complexity. With the aim of improving the performance of MPC by incorporating a modulation technique inside the MPC algorithm, the Modulated Model Predictive Control (M^2PC) concept has been introduced and applied to several power converter topologies [38]–[43]. In M^2PC, two or more switching states are selected by the cost function minimization algorithm and applied to the converter within a fixed switching cycle with appropriately chosen application times. In such way the switching frequency of M^2PC is kept constant, thus improving the waveform quality.

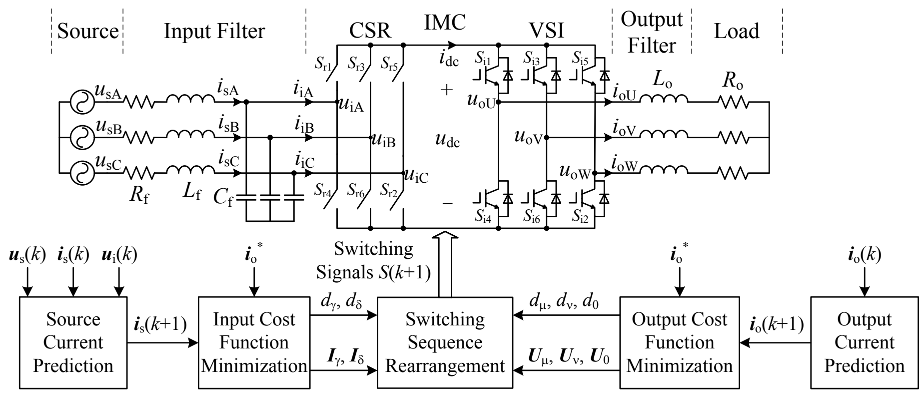

Fig.1 IMC System and Control Block Diagram of the Improved M^2PC

This paper presents the application of M^2PC for the IMC topology and it is organized as follow. Section II describes the operational proprieties of an IMC. The M^2PC design methodology adopted is presented in Section III. Finally, the simulation and experimental results are reported in Section IV and V, respectively.

II. CONVERTER DESCRIPTION

The IMC consists of a current source rectifier (CSR) and a voltage source inverter (VSI), as shown in Fig.1. The rectifier stage is composed of six bi-directional switches and it is coupled with the inverter stage by a common virtual DC-link.

For the rectifier stage, its output voltage $\boldsymbol{u_i}$ and DC-Link voltage u_{dc}, are defined by the switches state accordingly with the following expression

$$u_{\mathrm{dc}} = [S_{\mathrm{r1}} - S_{\mathrm{r4}} \quad S_{\mathrm{r3}} - S_{\mathrm{r6}} \quad S_{\mathrm{r5}} - S_{\mathrm{r2}}]\boldsymbol{u}_{\mathrm{i}} \tag{1}$$

where S_{ri} ($i \in \{1,2,3,4,5,6\}$) represents the switching state of the six switches in the rectifier stage, whose value is 1 or 0 for closed state and open state respectively. Correspondingly, the input current vector $\boldsymbol{i}_{\mathrm{i}}$ is calculated as in (2), where i_{dc} is the DC-Link current.

$$\boldsymbol{i}_{\mathrm{i}} = [S_{\mathrm{r1}} - S_{\mathrm{r4}} \quad S_{\mathrm{r3}} - S_{\mathrm{r6}} \quad S_{\mathrm{r5}} - S_{\mathrm{r2}}]^T i_{\mathrm{dc}} \tag{2}$$

Similarly, the inverter stage currents, $\boldsymbol{i_o}$, and voltages, $\boldsymbol{u_o}$, are defined as follows

$$i_{\mathrm{dc}} = [S_{\mathrm{i1}} - S_{\mathrm{i4}} \quad S_{\mathrm{i3}} - S_{\mathrm{i6}} \quad S_{\mathrm{i5}} - S_{\mathrm{i2}}]\boldsymbol{i}_{\mathrm{o}} \tag{3}$$

$$\boldsymbol{u}_{\mathrm{o}} = [S_{\mathrm{i1}} - S_{\mathrm{i4}} \quad S_{\mathrm{i3}} - S_{\mathrm{i6}} \quad S_{\mathrm{i5}} - S_{\mathrm{i2}}]^T u_{\mathrm{dc}} \tag{4}$$

where S_{ie} ($e \in \{1,2,3,4,5,6\}$) represents the switching state of the six switches in the inverter stage, whose values are 1 or 0, for closed state and open state respectively.

In order to properly operate the IMC requires a capacitive input filter on the CSR and an inductive output filter on the VSI. However in order to improve the waveforms quality usually LC filter are preferred.

For the safety operation of IMC, the following three conditions are mandatory to be met:

- Any two input phases cannot be short circuited.
- Any output phase cannot be open circuited.
- The DC-Link voltage must be positive.

According to these constraints, there are 9 valid switching states for the rectifier stage and 8 valid switching states for the inverter stage.

III. M^2PC DESIGN

As shown in Fig. 1, the M^2PC algorithm can be divided into five sections. Initially, source and output current prediction generate $\boldsymbol{i}_s(k+1)$ and $\boldsymbol{i}_o(k+1)$, which are the predicted input and output currents at the $(k+1)^{th}$ sampling instant. Then the input and output cost function minimization algorithms select which switching states are going to be applied at the input and output stage of the IMC. Finally, the switching sequence rearrangement allocates the time of each state applied to IMC. It can be seen in Fig. 1 that M^2PC selects two switching states for rectifier stage and three switching states for the inverter stage in one sampling period. This is a procedure, similar to PWM algorithms, while traditional MPC generates only one switching state for each stage, as presented in [31]. M^{2}PC is presented in details in the following subsections.

A. Input and Output Current Prediction

The discrete state-space equation for the input side, with source current $\boldsymbol{i}_s$ and input voltage $\boldsymbol{u}_i$ as state variables, is obtained from Fig. 1:

$$\begin{bmatrix} \boldsymbol{i}_s(k+1) \\ \boldsymbol{u}_i(k+1) \end{bmatrix} = \Phi_i \begin{bmatrix} \boldsymbol{i}_s(k) \\ \boldsymbol{u}_i(k) \end{bmatrix} + \Gamma_i \begin{bmatrix} \boldsymbol{u}_s(k) \\ \boldsymbol{i}_i(k) \end{bmatrix} \tag{5}$$

where matrices Φ_i and Γ_i are:

$$\Phi_i = e^{A_i T_s} \quad , \quad \Gamma_i = A_i^{-1}(\Phi_i - I)B_i \tag{6}$$

$$A_i = \begin{bmatrix} -{R_f}/{L_f} & -{1}/{L_f} \\ -{1}/{C_f} & 0 \end{bmatrix} \quad , \quad B_i = \begin{bmatrix} {1}/{L_f} & 0 \\ 0 & -{1}/{C_f} \end{bmatrix} \tag{7}$$

with L_f, R_f, and C_f representing the input filter parameters and T_s is the sampling time. Similarly, the discrete state-space equation for the output stage, having the output current $\boldsymbol{i}_o$ as the single state variable, is described as follows

$$\boldsymbol{i}_o(k+1) = \Phi_o \boldsymbol{i}_o(k) + \Gamma_o \boldsymbol{u}_o(k) \tag{8}$$

$$\Phi_o = e^{-\frac{R_o}{L_o}T_s} \quad , \quad \Gamma_o = -\frac{1}{R_o}(\Phi_o - 1) \tag{9}$$

where L_o and R_o represent the output filter inductance and load resistance, respectively. Equations (5) and (8) are used to predict the values of the state variables at the k+1 sampling instant and are calculated for every possible switching states of both rectifier and inverter stages.

B. Cost Function Minimization

The cost function g for each switching state is defined as the absolute square value of the input and output currents error:

$$g = |\boldsymbol{i}^* - \boldsymbol{i}(k+1)|^2 \tag{10}$$

This definition is suitable for all the switching states of both the rectifier stage and inverter stages. The input current reference is computed using a power balance method. The active power at the input side of the matrix converter [3] is defined as follows

$$P_i = \frac{3}{2}\left(I_s U_s \cos(\varphi_s) - R_f {I_s}^2\right) \tag{11}$$

where I_s and U_s are the modules of $\boldsymbol{i}_s$ and $\boldsymbol{u}_s$ respectively and φ_s is their corresponding phase shift. From the definitions of output active power

$$P_o = \frac{3}{2} R_o {I_o}^2 \tag{12}$$

and the converter efficiency

$$\mu = \frac{P_o}{P_i} \tag{13}$$

the reference source current module is computed as follows

$$I_s^* = \frac{U_s \cos(\varphi_s) \pm \Delta}{R_f} \quad , \quad \Delta = \sqrt{(U_s \cos(\varphi_s))^2 - \frac{4 {I_o^*}^2 R_f R_o}{\mu}} \tag{14}$$

where both the reference output current module I^*_o and phase φ_s are user defined. In fact, by imposing the current reference angle, it is possible to achieve reactive power control and, in regenerative configurations, reverse active power flow from the output stage to the rectifier stage. However, in the latter case, the source current reference has to be modified accordingly to the equations in [3].

M^{2}PC is first executed for the rectifier stage. In this stage, $g_{i\gamma}$ is defined as the cost function of one switching state $\boldsymbol{I}_\gamma$ and $g_{i\delta}$ as the cost function of the next adjacent switching state $\boldsymbol{I}_\delta$ (i.e. only one device commutation separates the states $\boldsymbol{I}_\gamma$ and $\boldsymbol{I}_\delta$). The values $g_{i\gamma}$ and $g_{i\delta}$ are calculated according to (10), considering the two states $\boldsymbol{I}_\gamma$ and $\boldsymbol{I}_\delta$ respectively. The cost function of the vectors couple is then defined as

$$g_i = d_{i\gamma} g_{i\gamma} + d_{i\delta} g_{i\delta} \tag{15}$$

where $d_{i\gamma}$ and $d_{i\delta}$ are the duty cycle associated with $\boldsymbol{I}_\gamma$ and $\boldsymbol{I}_\delta$ respectively. Assuming the duty cycles inversely proportional to the cost faction associated with the same vector, it is possible to define the following system

$$\begin{cases} d_{i\gamma} = \frac{k}{g_{i\gamma}} \\ d_{i\delta} = \frac{k}{g_{i\delta}} \\ d_{i\gamma} + d_{i\delta} = 1 \end{cases} \tag{16}$$

where k is a normalizing constant. Solving the system for $d_{i\gamma}$, $d_{i\delta}$ and k, it is possible to obtain

$$d_{i\gamma} = \frac{g_{i\delta}}{g_{i\gamma} + g_{i\delta}} \quad , \quad d_{i\delta} = \frac{g_{i\gamma}}{g_{i\gamma} + g_{i\delta}} \quad , \quad g_i = \frac{g_{i\gamma} g_{i\delta}}{g_{i\gamma} + g_{i\delta}} \tag{17}$$

The best couple of adjacent switching states $\boldsymbol{I}_\gamma$ and $\boldsymbol{I}_\delta$ of the rectifier stage is selected in order to minimize g_i as shown in (15), and then their duty cycles can be calculated using (17). From the control of the rectifier stage, the average DC-Link voltage required by the control of the inverter stage is also obtained:

$$u_{dc} = d_{i\gamma} u_{dc\gamma} + d_{i\delta} u_{dc\delta} \tag{18}$$

where $u_{dc\gamma}$ and $u_{dc\delta}$ are the DC-Link voltages obtained when state $\boldsymbol{I}_\gamma$ and $\boldsymbol{I}_\delta$ are applied to the rectifier stage separately.

Similarly, the inverter stage control is implemented defining the cost functions for two adjacent switching states $\boldsymbol{U}_\mu$ and $\boldsymbol{U}_\nu$ and the zero voltage state $\boldsymbol{U}_0$ according to (10), namely $g_{u\mu}$, $g_{u\nu}$, and g_{u0}. The cost function for the inverter stage is then defined as in (19), and the associated duty cycles of $\boldsymbol{U}_\mu$, $\boldsymbol{U}_\nu$, and $\boldsymbol{U}_0$ are calculated as in (20).

$$g_u = \frac{g_{u\mu} g_{u\nu} g_{u0}}{g_{u\mu} g_{u\nu} + g_{u\nu} g_{u0} + g_{u\mu} g_{u0}} \tag{19}$$

$$
\begin{cases}
d_{\mathrm{u}\mu} = \dfrac{g_{\mathrm{u}\nu} g_{\mathrm{u}0}}{g_{\mathrm{u}\mu} g_{\mathrm{u}\nu} + g_{\mathrm{u}\nu} g_{\mathrm{u}0} + g_{\mathrm{u}\mu} g_{\mathrm{u}0}} \\
d_{\mathrm{u}\nu} = \dfrac{g_{\mathrm{u}\mu} g_{\mathrm{u}0}}{g_{\mathrm{u}\mu} g_{\mathrm{u}\nu} + g_{\mathrm{u}\nu} g_{\mathrm{u}0} + g_{\mathrm{u}\mu} g_{\mathrm{u}0}} \\
d_{\mathrm{u}\nu} = \dfrac{g_{\mathrm{u}\mu} g_{\mathrm{u}\nu}}{g_{\mathrm{u}\mu} g_{\mathrm{u}\nu} + g_{\mathrm{u}\nu} g_{\mathrm{u}0} + g_{\mathrm{u}\mu} g_{\mathrm{u}0}} = 1 - d_{\mathrm{u}\mu} - d_{\mathrm{u}\nu}
\end{cases}
\tag{20}
$$

By minimizing g_{u} the best couple of adjacent switching states $\boldsymbol{U}_{\mu}$ and $\boldsymbol{U}_{\nu}$ for the inverter stage are selected, with the zero voltage state $\boldsymbol{U}_0$ selected to minimize the number of devices commutations.

The control of the inverter stage also generates the average DC-Link current i_{dc} to be used in the control of the rectifier stage. Even if i_{dc} can be calculated using a similar approach to the one in (18), it can also be expressed as in (21) in order to reduce the control computational burden

$$
i_{\mathrm{dc}} = \frac{P_{\mathrm{o}}^{*}}{u_{dc}} \tag{21}
$$

where u_{dc} is obtained by (18) and P_{o}^{*} is the reference value of the output active power, calculated as in (22) from the output current amplitude reference value I_{om}^{*}.

$$
P_{\mathrm{o}}^{*} = 1.5 R_{\mathrm{o}} (I_{\mathrm{om}})^2 \tag{22}
$$

Equation (22) is derived from power balance considerations on the IMC converter. In fact, since the IMC does not present any energy storage elements on the DC-Link, the input active power, DC-Link power, and output active power are always equal, assuming lossless power devices.

Since the control of the rectifier stage and the inverter stage are executed sequentially, one sample delay is present on the calculation of i_{dc}. In fact, while the value of u_{dc} is calculated by the rectifier stage controller and instantaneously applied to the inverter stage control, the value of i_{dc} is calculated by the inverter stage controller and applied to the rectifier stage control at the next sampling period. This approximation may degrade the input performances, even if its effect may be neglected for the considered sampling frequency.

C. Switching Pattern

Due to the absence of DC-Link energy storage elements, the switching sequences of the rectifier stage and inverter stage are coupled, in order to obtain the expected input and output currents. The switching pattern proposed in this paper is shown in Fig. 2. In this pattern, the switching sequences of the two stages are closely coordinated. The inverter stage application times are allocated proportionally to the rectifier stage application times, hence proportionally to $\boldsymbol{I}_{\gamma}$ in the first part of the switching cycle and to $\boldsymbol{I}_{\delta}$ in the second part of the switching cycle. The resulting duty cycles d_{V1}~d_{V6} associated with the states of the inverter stage are calculated as follows:

$$
\begin{cases}
d_{\mathrm{V1}} = {d_{\mathrm{u0}}}/{4} \\
d_{\mathrm{V2}} = d_{\mathrm{V1}} + d_{\mathrm{i}\gamma} d_{\mathrm{u}\mu} \\
d_{\mathrm{V3}} = d_{\mathrm{V2}} + d_{\mathrm{i}\gamma} d_{\mathrm{u}\nu} \\
d_{\mathrm{V4}} = d_{\mathrm{V3}} + 2 d_{\mathrm{V1}} \\
d_{\mathrm{V5}} = d_{\mathrm{V4}} + d_{\mathrm{i}\delta} d_{\mathrm{u}\nu} \\
d_{\mathrm{V6}} = d_{\mathrm{V5}} + d_{\mathrm{i}\delta} d_{\mathrm{u}\mu\mu}
\end{cases}
\tag{23}
$$

and the duty cycle d_{C} associated with the commutation of the rectifier stage is equal to

$$
d_{\mathrm{c}} = d_{\mathrm{V3}} + d_{\mathrm{V1}} \tag{24}
$$

TABLE I. SIMULATION PARAMETERS

Source	U_{s}=110V, f_{i}=60Hz
Input LC Filter	L_{f}=145μH, C_{f}=20μF, R_{f}=0.4Ω
Load	L_{o}=3mH, R_{o}=20Ω
Output Current Reference	I_{om}^{*}=4A, f_{o}=30Hz
Sampling Time	T_{s}=100μs

As it is shown in Fig. 2, the symmetrical switching pattern selected for this application results in a switching frequency which is two times the control sampling frequency, thus obtaining an improved waveform quality without increasing the control platform computational burden.

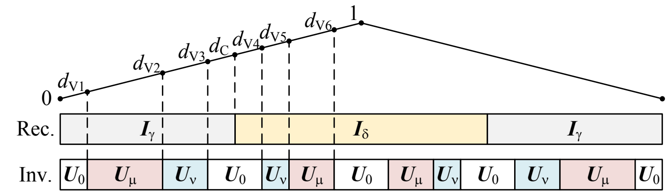

Fig. 2 Switching pattern

It is clear from (23) and (24) that d_{C} is always larger than d_{V3} and smaller than d_{V4}. Therefore, the rectifier stage commutation always happens when the DC-Link current i_{dc} is zero, i.e. when the zero voltage stage $\boldsymbol{U}_0$ is applied to the inverter stage. This means that zero-current switching is guaranteed for the rectifier stage, simplifying the commutation strategy of the IMC. In addition, similar to the switching pattern in conventional PWM algorithms [37], the inverter stage duty cycles are adjusted accordingly to the rectifier stage duty cycle. Only the average DC-Link voltage produced by the rectifier stage is required from for the inverter stage control, while the average DC-Link current produced by the inverter stage is required for the rectifier stage control. The selected switching pattern ensure that u_{dc} and i_{dc} can be considered constant during a sampling period, allowing independent control of the two stages and sinusoidal input and output currents waveforms. With respect to classical SVM strategies for IMC, in M^{2}PC the duty cycles are calculated using an empirical method based on the normalized cost function ratio for different switching states. The resulting duty cycles represent a sub-optimal solution which allows to obtain a predetermined switching pattern and, as a consequence, a fixed switching frequency whilst maintaining all the attractive features of MPC. It is shown in [40] that the resulting cost function of M^{2}PC always has a lower value than the equivalent for a classical MPC controller.

IV. SIMULATION RESULTS

Simulation using Matlab/Simulink have been carried out in order to compare the performance of the proposed M^{2}PC with the traditional MPC [26]. The parameters of the simulation model are shown in Table I.

The source currents and their FFT plots for the standard MPC and the proposed M^{2}PC are shown in Fig. 3. It is clear from Fig. 3 that $\boldsymbol{i}_s$ is severely distorted when using the traditional MPC working under a relatively low sampling frequency (10 kHz). Clearly by increasing the sampling frequency to 50 kHz the input current quality is increased. However, since predictive controllers are commonly demanding in terms of computational resources, it is not always possible to increase the sampling frequency in practical implementations. On the other hand, by using the proposed M^{2}PC, the THD of $\boldsymbol{i}_s$ is reduced to 12.53% with the harmonics content concentrated around multiples of the switching frequency and without the need of increasing the sampling frequency. Similar conclusions can be drawn from the waveforms of output current $\boldsymbol{i}_o$ and its FFT which are shown in Fig. 4. Compared with the traditional MPC, M^{2}PC helps to achieve better waveform quality also on the inverter stage, where the output currents THD is reduced to 7.55%. In addition, the waveforms of DC-Link voltage u_{dc} and current i_{dc} are shown in Fig. 5. The commutation of u_{dc} represents the switching state change of the rectifier stage. With the traditional MPC, it is possible for the rectifier stage to change its switching state when i_{dc} is nonzero. This may increase the converter losses and a more complex commutation strategy (e.g. four-step commutation) may be required for the rectifier stage. On the contrary, with M^{2}PC, the commutation of u_{dc} always occurs when i_{dc} is zero, ensuring zero-current switching of the rectifier stage.

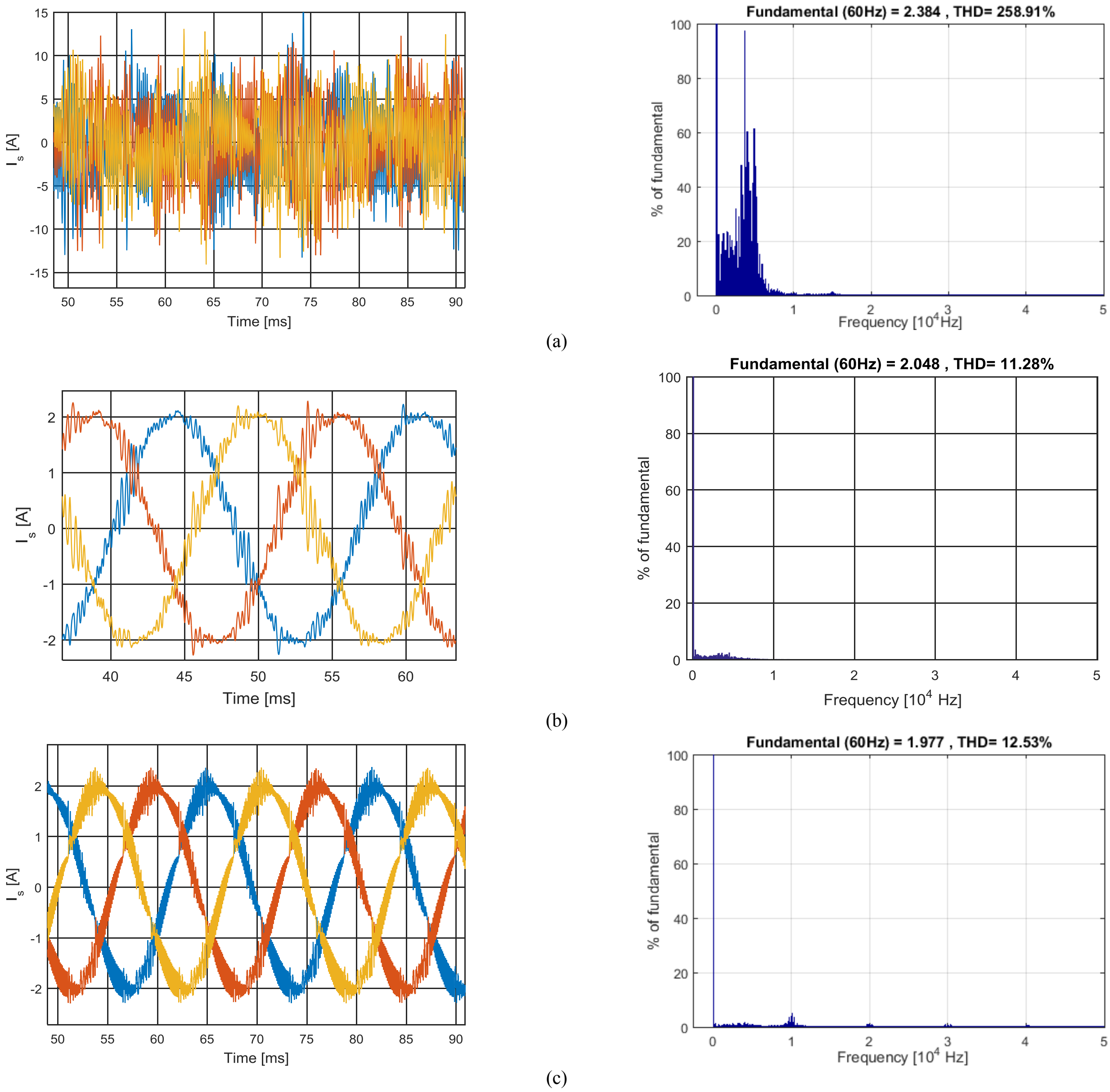

Fig. 3 Waveforms of source current $\boldsymbol{i}_s$ and its FFT: (a) with the traditional MPC operating at a sampling frequency of 10 kHz; (b) (a) with the traditional MPC operating at a sampling frequency of 50 kHz; (c) with M^{2}PC operating at a sampling frequency of 10 kHz.

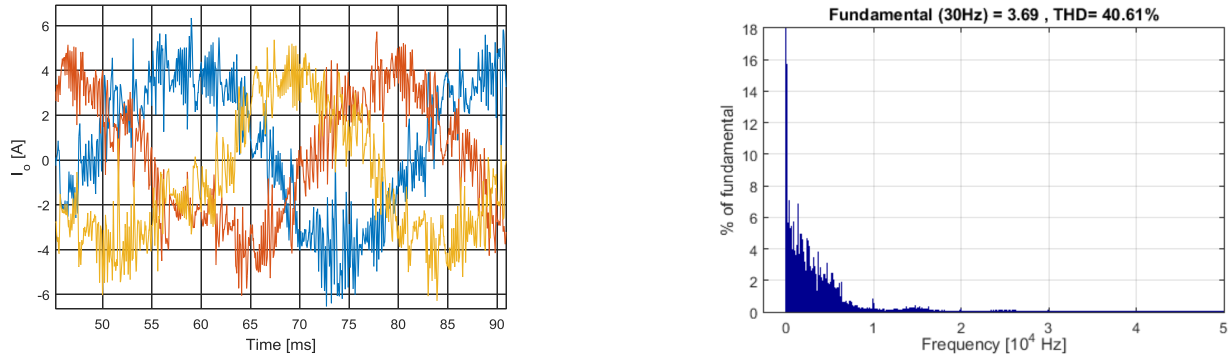

(a)

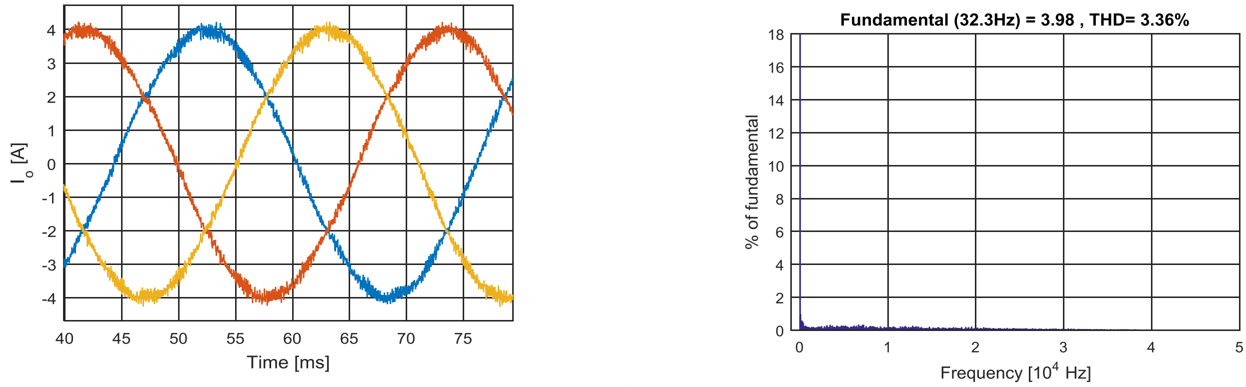

(b)

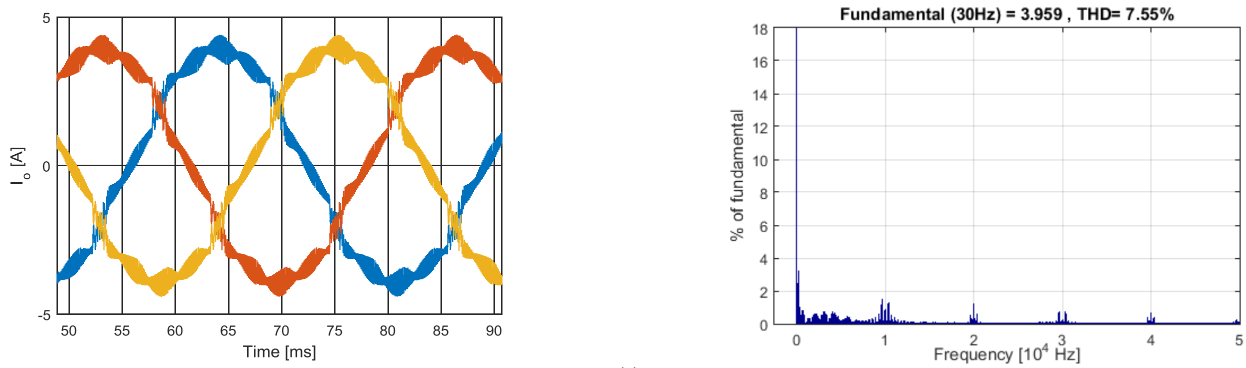

(c)

Fig. 4 Waveforms of output current $\boldsymbol{i_o}$ and its FFT: (a) with the traditional MPC operating at a sampling frequency of 10 kHz; (b) (a) with the traditional MPC operating at a sampling frequency of 50 kHz; (c) with M^{2}PC operating at a sampling frequency of 10 kHz..

V. Experimental Results

M^{2}PC is further evaluated experimentally on the prototype shown in Fig. 6. Experimental parameters match the simulation parameters shown in Table I.

In addition to the input filter, an EMI filter is connected to the AC source. Detailed information about the EMI filter design can found in [13]. The control scheme is implemented on a Spectrum Digital control board featuring a Texas Instruments C6713 DSP, coupled with a ProAsic 3 FPGA board.

Firstly, the control steady-state performances are evaluated for an output current reference of 4A amplitude and 30Hz frequency. The obtained experimental result is illustrated in Fig. 7. From Fig. 7 (a), it can be noted that the source current is in phase with the source voltage, providing unity power factor operation. Moreover, both the source current and output current are sinusoidal, with the harmonic spectrum shown in Fig. 7 (b) and Fig. 7 (c). By comparing Fig. 7 with Fig. 3, it can be concluded that source current and output current harmonic spectrum validate the simulation results. However, the output current first harmonic amplitude is 3.75A, presenting a steady state error of 6.25%. This is a common problem related with model based control techniques, where the system model inaccuracies result in a steady-state error on the controlled variables. Regarding the harmonic content of the source current around the sampling frequency (10kHz), it can be noted a discrepancy between simulation and experimental results. This difference is related to the EMI filter on the input side, which helps to attenuate the high-order harmonics around the switching frequency and it is not included in the discretized model used for control design.

In the second set of results, the output current frequency is set to 60Hz, while the other control parameters are kept as in the previous case. The obtained experimental result is shown in Fig. 8 where it can be noted that the source and output current harmonic distribution present minimal variation when the output current frequency varies, resulting in stable control performances for wide variations of the output current frequency.

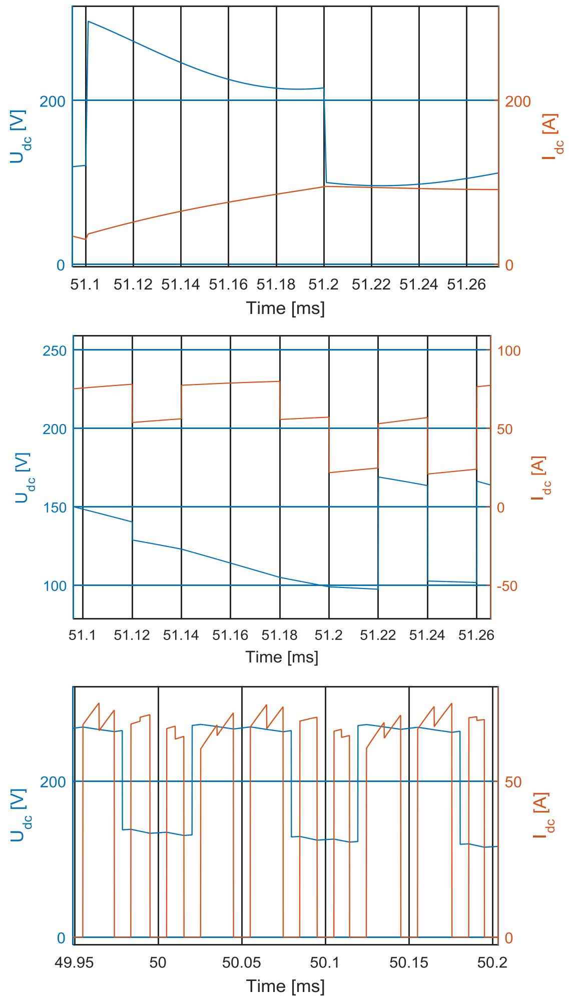

Fig. 5 Waveforms of DC-link voltage u_{dc} and current i_{dc}: (a) with the traditional MPC operating at a sampling frequency of 10 kHz; (b) (a) with the traditional MPC operating at a sampling frequency of 50 kHz; (c) with M^{2}PC operating at a sampling frequency of 10 kHz

Finally, the dynamic performances are evaluated with step changes of both output current amplitude and frequency. The results are shown in Fig. 9 and Fig. 10, respectively. As expected, the control presents a fast dynamic response on both input and output currents.

The output current frequency can be clearly increased, as it is limited mainly by the control sampling frequency (10kHz) and the output filters parameters. Considering the high control bandwidth of predictive controllers, the output current frequency could be increased up to its theoretical limit of half the sampling frequency without causing instability. However due to the reduced number of samples the results may not be acceptable in terms of current THD. For such reason, as it is commonly done with standard controller, a practical limit for the output frequency can be set at one tenth of the sampling frequency (1kHz).

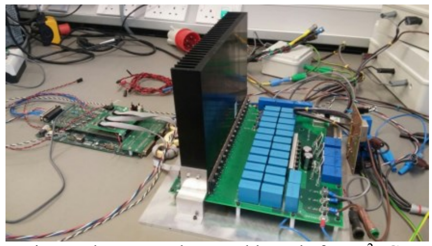

Fig. 6 IMC Experimental setup and control boards for M^{2}PC testing.

When the obtained results with M^{2}PC are compared with results obtained in other works, such as in [35], using a classical MPC controller, it can be noted that MPC can still obtain better performances of MPC when an higher sampling frequency is considered. However, this is not always possible since the high computational demand of MPC limits its application to relatively low sampling frequencies, such as 10kHz, or requires the use of costly high end control boards with higher clock frequency.

VI. Conclusion

A fixed switching frequency Finite-States Model Predictive Control, named Modulated Model Predictive Control (M^{2}PC) has been proposed in this paper for indirect matrix converters. M^{2}PC includes a suitable modulation scheme inside the control cost function minimization algorithm. In this case the switching pattern of a classical SVM for IMC , which requires the highest number of commutation, has been implemented. However other switching pattern are still applicable to M^{2}PC. Compared to the traditional MPC, the proposed approach has been demonstrated to have significant advantages. M^{2}PC combines the fast dynamic performances of MPC with the increased waveform quality of SVM. The results obtained shows that M^{2}PC is able to operate with low THD values with the same input and output filter parameters implemented when a SVM is considered. On the contrary MPC will require a much higher sampling frequency in order to achieve performance similar to M^{2}PC, which is not always possible due to the computational limitations of modern control boards. Moreover, zero-current switching of the rectifier stage is achieved, which benefits simplifying the commutation strategy of IMC in practical implementations and increase the converter efficiency. The control performance of M^{2}PC is also improved by obtaining sinusoidal supply currents and sinusoidal output currents with improved control accuracy.

The research results presented in this paper show that M^{2}PC represents an alternative solution to conventional PWM algorithms, when applied to the IMC and higher control bandwidth is required by the application. Both steady-state and dynamic performance of M^{2}PC are verified in simulation and validated with experimental results.

M^{2}PC retains all the desirable advantages of MPC, such as fast dynamic performance and multi-objective control. However the technique also has the advantages of using a PWM scheme, such as a fixed switching frequency and improved waveform quality without the need of a relatively high sampling frequency.

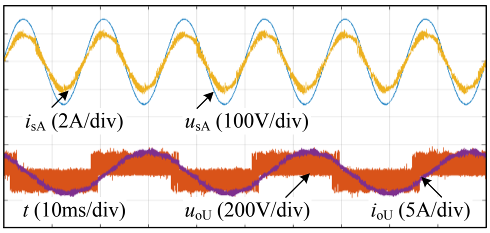

(a)

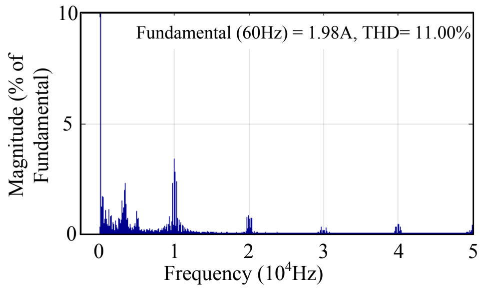

(b)

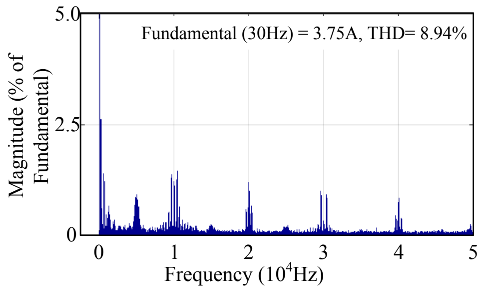

(c)

Fig. 7 Experimental results of IMC with the M^{2}PC, where output current amplitude reference is 4A and output frequency is 30Hz: (a) Waveforms of source voltage (u_{sA}), source current (i_{sA}), output line voltage (u_{oUV}), and output current (i_{oU}); (b) Spectrum distribution of i_{sA}; (c) Spectrum distribution of i_{oU}.

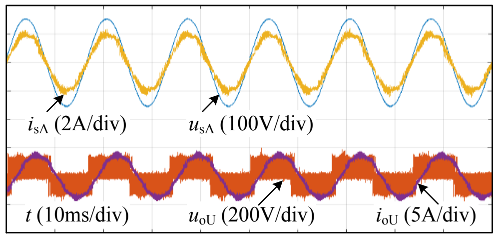

(a)

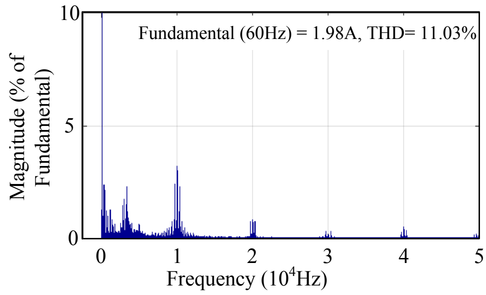

(b)

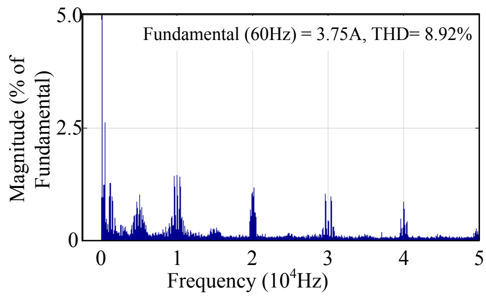

(c)

Fig. 8 Experimental results of IMC with the M^{2}PC, where output current amplitude reference is 4A and output frequency is 60Hz: (a) Waveforms of source voltage (u_{sA}), source current (i_{sA}), output line voltage (u_{oUV}), and output current (i_{oU}); (b) Spectrum distribution of i_{sA}; (c) Spectrum distribution of i_{oU}.

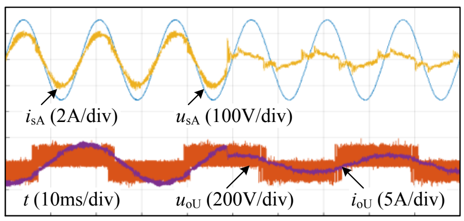

(a)

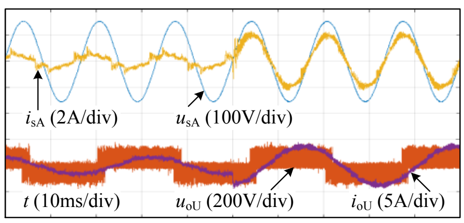

(b)

Fig. 9 Experimental results of IMC with the M^{2}PC, where the reference value I_{om}^* of output current amplitude reference steps between 2A and 4A and output frequency keeps at 30Hz: (a) I_{om}^* steps from 4A down to 2A; (b) I_{om}^* steps from 2A up to 4A.

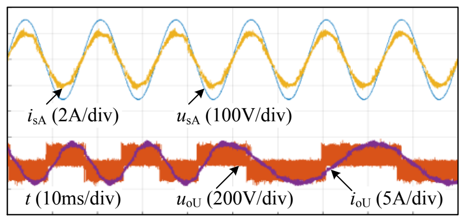

(a)

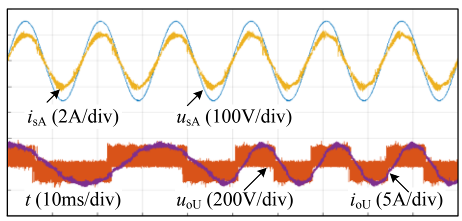

(b)

Fig. 10 Experimental results of IMC with the M^{2}PC, where the output frequency f_o steps between 30Hz and 60Hz and the output current amplitude reference keeps at 4A: (a) f_o steps from 60Hz down to 30Hz; (b) f_o steps from 30Hz up to 60Hz.

References

[1] T. Friedli, J. W. Kolar, J. Rodriguez, and P. W. Wheeler, "Comparative evaluation of three-phase AC-AC matrix converter and voltage DC-link back-to-back converter systems," *IEEE Trans. Ind. Electron.*, vol. 59, no. 12, pp. 4487–4510, 2012.

[2] P. W. Wheeler, J. Rodriguez, J. C. Clare, L. Empringham, and A. Weinstein, "Matrix converters: a technology review," *IEEE Trans. Ind. Electron.*, vol. 49, no. 2, pp. 276–288, 2002.

[3] A. Formentini, A. Trentin, M. Marchesoni, P. Zanchetta, and P. Wheeler, "Speed Finite Control Set Model Predictive Control of a PMSM Fed by Matrix Converter," *IEEE Trans. Ind. Electron.*, vol. 62, no. 11, pp. 6786–6796, 2015.

[4] L. Rovere, A. Formentini, A. Gaeta, P. Zanchetta, and M. Marchesoni, "Sensorless Finite Control Set Model Predictive Control for IPMSM Drives," *IEEE Trans. Ind. Electron.*, vol. 63, no. 9, pp. 5921–5931, 2016.

[5] S. Lopez Arevalo, P. Zanchetta, P. W. Wheeler, A. Trentin, and L. Empringham, "Control and Implementation of a Matrix-Converter-Based AC Ground Power-Supply Unit for Aircraft Servicing," *IEEE Trans. Ind. Electron.*, vol. 57, no. 6, pp. 2076–2084, 2010.

[6] N. Xuan Bac, D. M. Vilathgamuwa, and U. K. Madawala, "A SiC-Based Matrix Converter Topology for Inductive Power Transfer System," *IEEE Trans. Power Electron.*, vol. 29, no. 8, pp. 4029–4038, 2014.

[7] M. Moghaddami, A. Anzalchi, and A. I. Sarwat, "Single-Stage Three-Phase AC-AC Matrix Converter for Inductive Power Transfer Systems," *IEEE Trans. Ind. Electron.*, vol. 63, no. 10, pp. 6613–6622, 2016.

[8] S. Weerassinghe, U. K. Madawala, and D. J. Thrimawithana, "A Matrix Converter based Bidirectional Contactless Grid Interface," *IEEE Trans. Power Electron.*, vol. 32, no. 3, pp. 1–12, 2016.

[9] S. F. Pinto, P. Alcaria, J. Monteiro, and J. F. Silva, "Matrix Converter-Based Active Distribution Transformer," *IEEE Trans. Power Del.*, vol. 31, no. 4, pp. 1493–1501, 2016.

[10] P. Szczesniak and J. Kaniewski, "Hybrid Transformer with Matrix Converter," *IEEE Trans. Power Del.*, vol. 31, no. 3, pp. 1388–1396, 2016.

[11] L. Wei and T. a. Lipo, "A novel matrix converter topology with simple commutation," *Conf. Rec. 2001 IEEE Ind. Appl. Conf. 36th IAS Annu. Meet. (Cat. No.01CH37248)*, vol. 3, pp. 1749–1754, 2001.

[12] J. W. Kolar, T. Friedli, J. Rodriguez, and P. W. Wheeler, "Review of three-phase PWM AC-AC converter topologies," *IEEE Trans. Ind. Electron.*, vol. 58, no. 11, pp. 4988–5006, 2011.

[13] A. Trentin, L. Empringham, L. De Lillo, P. Zanchetta, P. Wheeler, and J. Clare, "Experimental comparison of a direct matrix converter using Si IGBT and SiC MOSFETs," *IEEE Trans. Ind. Appl.*, vol. 52, no. 5, pp. 4135–4145, 2016.

[14] L. Empringham, J. W. Kolar, J. Rodriguez, P. W. Wheeler, and J. C. Clare, "Technological issues and industrial application of matrix converters: A review," *IEEE Trans. Ind. Electron.*, vol. 60, no. 10, pp. 4260–4271, 2013.

[15] K. Koiwa and J.-I. Itoh, "A Maximum Power Density Design Method for Nine Switches Matrix Converter Using SiC-MOSFET," *IEEE Trans. Power Electron.*, vol. 31, no. 2, pp. 1189–1202, 2016.

[16] L. Wei, T. A. Lipo, and R. A. Lukaszewski, "Comparison of IGBT Cycling Capabilities for Different AC/AC Topologies," *IEEE Trans. Ind. Appl.*, vol. 46, no. 6, pp. 2475–2483, 2010.

[17] A. Trentin, L. de Lillo, L. Empringham, P. Zanchetta, P. Wheeler, and J. Clare, "Experimental Comparison of Device Thermal Cycling in Direct Matrix Converter (DMC) and Indirect Matrix Converter (IMC) using SiC MOSFETs," *IEEE Energy Convers. Congr. Expo.*, 2016.

[18] J. Lei, B. Zhou, X. Qin, J. Wei, and J. Bian, "Active damping control strategy of matrix converter via modifying input reference currents," *IEEE Trans. Power Electron.*, vol. 30, no. 9, pp. 5260–5271, 2015.

[19] J. Lei, B. Zhou, J. Bian, X. Qin, and J. Wei, "A Simple Method for Sinusoidal Input Currents of Matrix Converter Under Unbalanced Input Voltages," *IEEE Trans. Power Electron.*, vol. 31, no. 1, pp. 21–25, 2016.

[20] J. Rodriguez, M. Rivera, J. W. Kolar, and P. W. Wheeler, "A review of control and modulation methods for matrix converters," *IEEE Trans. Ind. Electron.*, vol. 59, no. 1, pp. 58–70, 2012.

[21] L. Zarri, M. Mengoni, A. Tani, and J. O. Ojo, "Range of the linear modulation in matrix converters," *IEEE Trans. Power Electron.*, vol. 29, no. 6, pp. 3166–3178, 2014.

[22] D. Casadei, G. Serra, A. Tani, and L. Zarri, "Matrix converter modulation strategies: A new general approach based on space-vector representation of the switch state," *IEEE Trans. Ind. Electron.*, vol. 49, no. 2, pp. 370–381, 2002.

[23] D. Casadei, G. Serra, A. Tani, and L. Zarri, "Optimal use of zero vectors for minimizing the output current distortion in matrix converters," *IEEE Trans. Ind. Electron.*, vol. 56, no. 2, pp. 326–336, 2009.

[24] M. Hamouda, H. F. Blanchette, and K. Al-Haddad, "Indirect matrix converters enhanced commutation method," *IEEE Trans. Ind. Electron.*, vol. 62, no. 2, pp. 671–679, 2015.

[25] X. Li, Y. Sun, J. Zhang, M. Su, and H. Shoudao, "Modulation Methods for Indirect Matrix Converter Extending the Input Reactive Power Range," *IEEE Trans. Power Electron.*, vol. 32, no. 6, pp. 1–1, 2016.

[26] M. Rivera, J. Rodriguez, J. R. Espinoza, and H. Abu-Rub, "Instantaneous reactive power minimization and current control for an indirect matrix converter under a distorted AC supply," *IEEE Trans. Ind. Informat.*, vol. 8, no. 3, pp. 482–490, 2012.

[27] M. López, J. Rodriguez, C. Silva, and M. Rivera, "Predictive Torque Control of a Multidrive System Fed by a Dual Indirect Matrix Converter," *IEEE Trans. Ind. Electron.*, vol. 62, no. 5, pp. 2731–2741, 2015.

[28] M. Rivera, J. Rodriguez, B. Wu, J. R. Espinoza, and C. a. Rojas, "Current control for an indirect matrix converter with filter resonance mitigation," *IEEE Trans. Ind. Electron.*, vol. 59, no. 1, pp. 71–79, 2012.

[29] T. Peng, H. Dan, J. Yang, H. Deng, Q. Zhu, W. Chunseng, G. Wihua, and J. Guerrero, "Open-Switch Fault Diagnosis and Fault Tolerant for Matrix Converter with Finite Control Set-Model Predictive Control," *IEEE Trans. Ind. Electron.*, vol. 63, no. January, pp. 5953–5963, 2016.

[30] M. Jussila and H. Tuusa, "Comparison of Simple Control Strategies of Space-Vector Modulated Indirect Matrix Converter Under Distorted Supply Voltage," *IEEE Trans. Power Electron.*, vol. 22, no. 1, pp. 139–148, 2007.

[31] S. Kouro, P. Cortés, R. Vargas, U. Ammann, and J. Rodríguez, "Model predictive control—A simple and powerful method to control power converters," *IEEE Trans. Ind. Electron.*, vol. 56, no. 6, pp. 1826–1838, 2009.

[32] A. Formentini, L. de Lillo, M. Marchesoni, A. Trentin, P. Wheeler, and P. Zanchetta, "A new mains voltage observer for PMSM drives fed by matrix converters," in *European Conference on Power Electronics and Applications (EPE)*, 2014, pp. 1–10.

[33] H. a. Young, M. a. Perez, J. Rodriguez, and H. Abu-Rub, "Assessing finite-control-set model predictive control: A comparison with a linear current controller in two-level voltage source inverters," *IEEE Ind. Electron. Mag.*, vol. 8, no. March, pp. 44–52, 2014.

[34] T. Geyer, N. Oikonomou, G. Papafotiou, and F. D. Kieferndorf, "Model Predictive Pulse Pattern Control," *IEEE Trans. Ind. Appl.*, vol. 48, no. 2, pp. 663–676, 2012.

[35] P. Correa, J. Rodríguez, M. Rivera, J. R. Espinozav, and J. W. Kolar, "Predictive control of an indirect matrix converter," *IEEE Trans. Ind. Electron.*, vol. 56, no. 6, pp. 1847–1853, 2009.

[36] J. Lei, B. Zhou, J. Wei, J. Bian, Y. Zhu, J. Yu, and Y. Yang, "Predictive Power Control of Matrix Converter with Active Damping Function," *IEEE Trans. Ind. Electron.*, vol. 63, no. 7, pp. 4550–4559, 2016.

[37] S. Kwak, S. E. Kim, and J. C. Park, "Predictive Current Control Methods with Reduced Current Errors and Ripples for Single-Phase Voltage Source Inverters," *IEEE Trans. Ind. Informat.*, vol. 11, no. 5, pp. 1006–1016, 2015.

[38] L. Tarisciotti, P. Zanchetta, A. Watson, J. C. Clare, M. Degano, and S. Bifaretti, "Modulated Model Predictive Control for a Three-Phase Active Rectifier," *IEEE Trans. Ind. Appl.*, vol. 51, no. 2, pp. 1610–1620, 2015.

[39] L. Tarisciotti, P. Zanchetta, A. Watson, P. Wheeler, J. C. Clare, and S. Bifaretti, "Multiobjective Modulated Model Predictive Control for a Multilevel Solid-State Transformer," *IEEE Trans. Ind. Appl.*, vol. 51, no. 5, pp. 4051–4060, 2015.

[40] L. Tarisciotti, P. Zanchetta, A. Watson, J. Clare, and S. Bifaretti, "Modulated Model Predictive Control for a 7-Level Cascaded H-Bridge back-to-back Converter," *IEEE Trans. Ind. Electron.*, vol. 61, no. 10, pp. 5375–5383, 2014.

[41] L. Tarisciotti, P. Zanchetta, A. J. Watson, J. C. Clare, M. Degano, and S. Bifaretti, “Modulated Model Predictve Control (M2PC) for a 3-Phase Active Front-End,” in *IEEE Energy Conversion Congress and Exposition (ECCE)*, 2013, pp. 1062–1069.

[42] L. Tarisciotti, A. Formentini, A. Gaeta, M. Degano, P. Zanchetta, R. Rabbeni, and M. Pucci, “Model Predictive control for Shunt Active Filters with Fixed Switching Frequency,” *IEEE Trans. Ind. Appl. Ind. Appl.*, vol. 9994, no. c, pp. 1–1, 2016.

[43] J. Lei, L. Tarisciotti, A. Trentin, P. Zanchetta, P. Wheeler, and A. Formentini, “Fixed Frequency Finite-State Model Predictive Control for Indirect Matrix Converters with Optimal Switching Pattern,” *IEEE Energy Convers. Congr. Expo.*, 2016.

Luca Tarisciotti (S’12-M’15) received the Master’s degree in electronic engineering from The University of Rome "Tor Vergata" in 2009 and his Ph.D. degree in Electrical and Electronic Engineering from the PEMC group, University of Nottingham in 2015. He is currently working as Research Fellow at the University of Nottingham, UK. His research interests includes matrix converters, DC/DC converters, multilevel converters, advanced modulation schemes, and advanced power converter control.

Jiaxing Lei (S’ 14) was born in Dazhou, China, 1991. He received B.S. degree in 2012 in Nanjing University of Aeronautics and Astronautics, Nanjing, China, where he is currently working toward the Ph.D. degree since 2012. From Sep. 2015 to Sep. 2016, he was a visiting scholar in the University of Nottingham. His main research interests are in matrix converters and its applications.

Andrea Formentini was born in Genova, Italy, in 1985. He received the M.S. degree in computer engineering and the PhD degree in electrical engineering from the University of Genova, Genova, in 2010 and 2014 respectively. He is currently working as research fellow in the Power Electronics, Machines and Control Group, University of Nottingham. His research interests include control systems applied to electrical machine drives and power converters.

Andrew Trentin received the “Laurea” and Ph.D. degrees in electrical engineering from the University of Bologna, Bologna, Italy, in 2001 and 2005, respectively. Since 2005, he has been a Research Fellow with The University of Nottingham, Nottingham, U.K. His current research interests are in the fields of electrical drives and direct ac/ac matrix converters for aircraft and automotive applications.

Pericle Zanchetta M’00 SM’15 received his MEng degree in Electronic Engineering and his Ph.D. in Electrical Engineering from the Technical University of Bari (Italy) in 1993 and 1997 respectively. In 1998 he became Assistant Professor of Power Electronics at the same University. In 2001 he became lecturer in control of power electronics systems in the PEMC research group at the University of Nottingham – UK, where he is now Professor in Control of Power Electronics systems. He has published over 260 peer reviewed papers and he is Chair of the IAS Industrial Power Converter Committee IPCC. His research interests include control of power converters and drives, Matrix and multilevel converters.

Prof Pat Wheeler received his BEng [Hons] degree in 1990 from the University of Bristol, UK. He received his PhD degree in Electrical Engineering for his work on Matrix Converters from the University of Bristol, UK in 1994. In 1993 he moved to the University of Nottingham and worked as a research assistant in the Department of Electrical and Electronic Engineering. In 1996 he became a Lecturer in the Power Electronics, Machines and Control Group at the University of Nottingham, UK. Since January 2008 he has been a Full Professor in the same research group. He is currently Head of the Department of Electrical and Electronic Engineering at the University of Nottingham. He is an IEEE PELs ‘Member at Large’ and an IEEE PELs Distinguished Lecturer. He has published 400 academic publications in leading international conferences and journals.

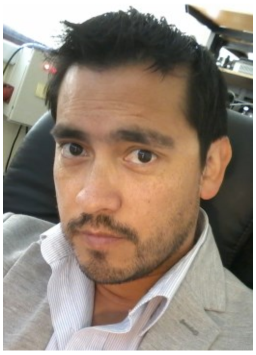

Marco Rivera (S'09-M'11) received his B.Sc. in Electronics Engineering and M.Sc. in Electrical Engineering from the Universidad de Concepcion, Chile, in 2007 and 2008, respectively. He received his PhD degree from the Department of Electronics Engineering, Universidad Tecnica Federico Santa Maria, in Valparaiso, Chile, in 2011 with a scholarship from the Chilean Research Fund CONICYT. During 2011 and 2012, Prof. Rivera held a Post Doctoral position and worked as part-time professor of Digital Signal Processors and Industrial Electronics at Universidad Tecnica Federico Santa Maria. Currently he is an Associate Professor in the Faculty of Engineering at Universidad de Talca, Curicó, Chile. Prof. Rivera Abarca was awarded a scholarship from the Marie Curie Host Fellowships for early stage research training in electrical energy conversion and conditioning technology at the University College Cork, Cork, Ireland in 2008. In 2012, Prof. Rivera was awarded the Chilean Academy of Science Doctoral Thesis Award (Premio Tesis de Doctorado Academia Chilena de Ciencias), for the best PhD thesis published in 2011, selected from among all national and international students enrolled in any exact or natural sciences program in Chile and also he was awarded as an Outstanding Engineer in 2015. His research interests include matrix converters, predictive and digital controls for high-power drives, four-leg converters, renewable energies and development of high performance control platforms based on Field-Programmable Gate Arrays.